Journal of Applied Physics ARTICLE scitation.org/journal/jap

Molecular dynamics simulations of the effect of dislocations on the thermal conductivity of iron

Cite as: J. Appl. Phys. **127**, 045106 (2020); doi: 10.1063/1.5127037
Submitted: 12 September 2019 · Accepted: 9 January 2020 ·
Published Online: 28 January 2020

Yandong Sun,[1] Yanguang Zhou,[2] Jian Han,[3] Ming Hu,[4,a)] Ben Xu,[1,3,b)] and Wei Liu[1,c)]

AFFILIATIONS

[1]Laboratory of Advanced Materials, School of Materials Science and Engineering, Tsinghua University, Beijing 100084, People's Republic of China
[2]Department of Mechanical and Aerospace Engineering, University of California Los Angeles, Los Angeles, California 90095, USA
[3]State Key Laboratory of New Ceramics and Fine Processing, School of Materials Science and Engineering, Tsinghua University, Beijing 100084, People's Republic of China
[4]Department of Mechanical Engineering, University of South Carolina, Columbia, South Carolina 29208, USA

[a)]hu@sc.edu
[b)]**Author to whom correspondence should be addressed:** xuben@mail.tsinghua.edu.cn
[c)]liuw@mail.tsinghua.edu.cn

ABSTRACT

Phonons contribute an appreciable proportion of the thermal conductivity of iron-based structural materials used in the nuclear industry. The decrease in thermal conductivity caused by defects such as dislocations will decrease the efficiency of nuclear reactors or lead to melting failure under transient heat flow. However, the phonon–dislocation scattering rate in iron is unknown, and the details of the scattering process have not been well studied. In this paper, the effect of dislocations on lattice thermal conductivity in pure iron is studied using molecular dynamics simulations. The temperature distribution in the neighborhood of the dislocation, the spectral heat flux, and the frequency-dependent phonon mean free paths are obtained. From a comparison with the results for a perfect crystal, we find that the dislocation can significantly decrease the lattice thermal conductivity. By using an average phonon group velocity, the phonon–dislocation scattering rate under a given dislocation density is obtained from the phonon mean free paths. Moreover, eigenmode analysis of a dislocation dipole model indicates that the phonons have a certain degree of localization, which reduces their ability to transport heat. Our study reveals the details of the phonon–dislocation scattering process and may help to interpret the reduced thermal conductivity caused by the dislocations that are generated during the service lives of iron-based structural materials.

I. INTRODUCTION

Iron-based materials are among the most important structural materials in the nuclear industry. For example, stainless steel is used as a structural material in the cores of fission reactors and for primary piping, and oxide dispersion-strengthened steel (ODS) will be used as nuclear fuel cladding material in the future.[1] In both fission and fusion reactors, these materials are subjected to a combination of high radiation dose and intense heat flux, leading to the generation of radiation defects such as vacancies, dislocation loops, and clusters.[1] Defects greatly reduce the thermal conductivity κ of the materials,[2] which decreases the efficiency of heat transfer from the primary coolant to the cooling water and potentially leads to melting failure of fuel rods under a heat flux of 1 MW/m^2. In solids, heat is carried mainly by electrons and phonons, and κ is a function of both the velocities and mean free paths (MFPs) of these carriers.[3] By scattering phonons and thereby reducing their MFPs, defects reduce the phonon contribution to the thermal conductivity, κ_L. Usually, mobile free electrons dominate the κ of metals according to the Wiedemann–Franz law.[3] However, in ferromagnetic iron, the MFPs of electrons decrease sharply owing to spin disorder, as a result of which parallel phonon conduction makes a greater contribution to κ.[4] Williams *et al.*[5] obtained κ_L at 300 K by fitting the experimental data for binary iron-based alloys and found that the lattice conductivity contributed 20%–40% of κ. Thus, a full understanding

of phonon scattering by defects is of great practical significance for the thermal control of iron-based nuclear materials.

Moreover, phonon–defect scattering has always been of great interest from a theoretical point of view. There have been a number of detailed studies of phonon scattering by point defects and interfaces,[6–10] but there is limited information available on phonon scattering by dislocations. Experimental studies have indicated that the presence of dislocations can reduce κ_L.[11–15] However, phonon–dislocation scattering rates have usually been calculated using a semi-empirical formula based on the Debye model, which is far from providing an understanding of the physical mechanism behind the experimental results. Computational methods offer a good approach to the study of phonon–dislocation scattering. Using molecular dynamics (MD) simulations, Xiong *et al.*[16] and Ni *et al.*[17] revealed that the anharmonicity arising from a highly distorted screw dislocation core leads to phonon scattering in silicon and silicon carbide, respectively. Termentzidis *et al.*[18] studied the variations in phonon–dislocation scattering among different types of dislocations, core structures, dislocation densities, and temperatures, thereby providing very rich information about the phonon–dislocation scattering process. Using an *ab initio* approach, Wang *et al.*[19] developed a method based on Green's functions to measure the phonon–dislocation scattering rate at realistic dislocation concentrations. Recent theoretical work has provided new insights into the phonon–dislocation scattering process. Li *et al.*[20] showed that the dislocation strain can be seen as a quasiparticle that can undergo inelastic collisions with phonons. Hanus *et al.*[21] found that phonon–dislocation scattering was closely related to the spacing between dislocations. However, in spite of these advances, a detailed understanding of phonon–dislocation scattering is still lacking.

In this paper, we perform nonequilibrium molecular dynamics (NEMD) simulations to study phonon transport across a virtual interface including an edge dislocation in a bcc iron crystal. A comparison is made between the dislocation model (D model) and the corresponding perfect model (P model, without dislocation). First, the temperature distribution along the heat flux direction is obtained directly from the NEMD simulations. Next, the frequency-dependent heat flux is investigated using our recently proposed frequency-domain direct decomposition method (FDDDM).[22–24] Then, phonon MFPs are fitted according to the length-dependent spectral heat flux calculated by performing NEMD simulations in models with different lengths. Finally, the eigenmodes of a dislocation dipole model are analyzed.

II. METHOD

A. Nonequilibrium molecular dynamics

The model contains 349 100 atoms arranged in a bcc structure (lattice parameter $a = 2.867$ Å at 20 K) with crystal orientation $\vec{u}_x = [100]$, $\vec{u}_y = [010]$, $\vec{u}_z = [001]$; see Fig. 1(a). It is 57.1 nm long in the x direction and has a cross section of $8.6 \times 8.6\,\text{nm}^2$. Two dislocations are embedded in the model: one is at the center of the model with Burgers vector $\langle 100 \rangle$ and the other in the corner of the model with Burgers vector $\langle \bar{1}00 \rangle$. The dislocation line is $\langle 001 \rangle$ for both dislocations. The dislocation density is $4 \times 10^{15}\,\text{m}^{-2}$. Since the dislocations are far away from each other, they can be considered

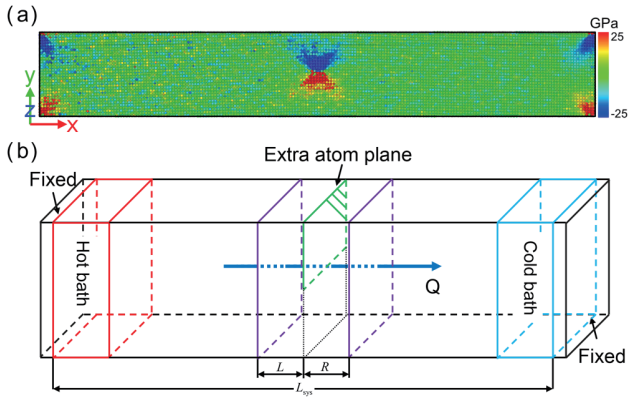

FIG. 1. (a) Dislocation model and (b) schematic of the cell used in the NEMD simulations.

isolated and the interaction between them can be neglected. Furthermore, the model is periodic in all directions.

A schematic of the cell used in the NEMD simulations is shown in Fig. 1(b). Both ends of the system are fixed by not including time integration in the MD simulation to prevent it from undergoing translational movements. Next to the fixed boundaries, atoms within a length $L_{\text{bath}} = 2$ nm are coupled to Langevin heat baths. The temperature is set to 40 K in the hot bath and 0.1 K in the cold bath. The selected temperature is low because we are trying to weaken the normal process (N-process) and Umklapp process (U-process), which usually cause large disturbances in the analysis of the phonon–dislocation scattering.[3] Two groups of atoms within 1.6 nm of the extra atom plane of the edge dislocation (denoted by **L** and **R**) are selected, and their velocities are sampled at successive time steps and will be used to calculate the spectral heat flux. The same procedure is performed for the P model. The NEMD simulations are carried out in the LAMMPS software package[25] with a time step of 5 fs. An embedded atom (EAM) potential taken from Ref. 26 is used to model the interactions between atoms. We perform 5.3×10^6 NEMD steps, corresponding to a total running time of 26.5 ns. The first 10 ns is used to relax the structure in isothermal–isobaric ensemble (NPT) and canonical ensemble (NVT), then the following 15 ns is used to obtain a steady temperature gradient and heat flux in a microcanonical ensemble (NVE), and, finally, the temperature distribution and the velocity for the FDDDM calculation are obtained in the last 1.5 ns.

B. Eigenmode analysis method

We also construct a dislocation dipole model containing 1128 atoms with 48-, 48-, and 2-atom layers in the x, y, and z directions, respectively, as shown in Fig. 2(a). The corresponding perfect model is shown in Fig. 2(b). The models are first relaxed using MD in the LAMMPS package[25] with isothermal–isobaric ensemble (NPT) and canonical ensemble (NVT), and then an energy minimization is applied. The final structures are used to calculate the phonon density of states (DOS) and eigenmodes using Phonopy software.[27] First, the

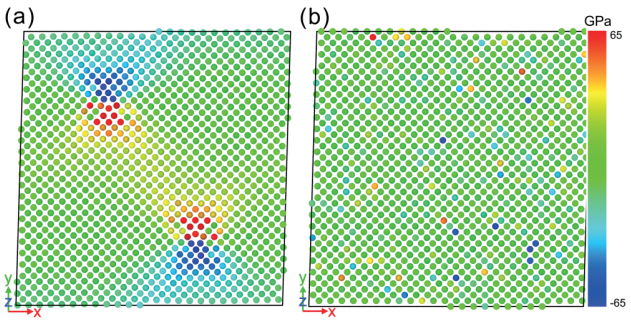

FIG. 2. (a) Dislocation dipole model and (b) corresponding perfect model used in the eigenmode analysis.

POSCAR files with displacement are generated by Phonopy, and the files are converted into LAMMPS data files. Then, the second-order interatomic force constants (IFCs) are obtained from the MD force calculation, and the force constants are converted back to Phonopy FORCE_SET file. Finally, the phonon DOS and eigenmodes of atoms can be obtained from Phonopy.

III. RESULT

A. Temperature distribution

The temperature distribution along the heat flux direction of the P and D models is obtained directly from the MD simulations (see Fig. 3). A perfect linear temperature distribution is obtained in the P model, but a temperature drop by about 2.1 K appears in the D model in the dislocation region. The gradient of the temperature is inversely proportional to the κ of the material, so the κ of the D model decreases.

Three regions are selected to calculate the heat flux: one is near the hot bath (H-R), another is in the dislocation region (D-R), and the third is near the cold bath (C-R). The heat flux is a vector with three components J_x, J_y, and J_z. The results are shown in Table I. Compared with the P model, J_x decreases and J_y is generated in the D model, which is due to the heat flux along the x direction being diverted into the y direction by the dislocation.

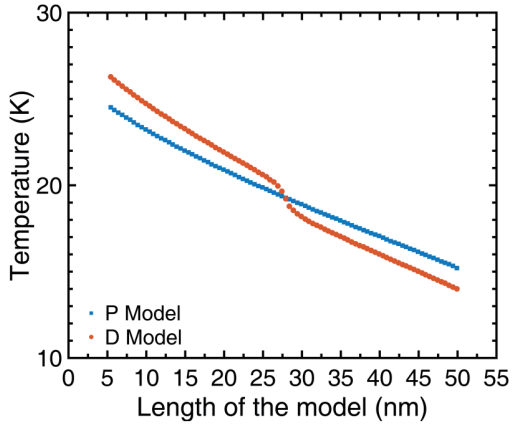

FIG. 3. Temperature distribution along the heat flux direction in the P model (blue) and the D model (red).

κ_L is calculated from Fourier's law

$$\kappa_L = -\frac{J_Q}{\partial T/\partial x}, \tag{1}$$

where J_Q is the time-averaged heat flux obtained directly from the NEMD simulation and $\partial T/\partial x$ is the temperature gradient of the entire system. The results are shown in Table II. κ_L is reduced by 18.6% in the D model owing to the presence of the dislocations.

In the classical MD simulation, since each phonons is equally populated,[28] the low-temperature MD results reported herein can predict the correct trend of transport behaviors of phonons. Moreover, the scattering rate of phonon–dislocation scattering will not change with temperature according to the theoretical equations

$$\tau_{DC}^{-1} = N_D \frac{\overline{V}^{4/3}}{v^2}\omega^3, \tag{2}$$

where τ_{DC}^{-1} is the scattering rate from the dislocation core, N_D is the dislocation density, $\overline{V}$ is the volume per atom, v is the average sound velocity, and ω is the phonon frequency,

$$\tau_{DS}^{-1} = 0.06 \times B_D^2 N_D \gamma^2 \omega \times \left\{\frac{1}{2} + \frac{1}{24}\left(\frac{1-2\nu}{1-\nu}\right)^2\left[1+\sqrt{2}\left(\frac{v_L}{v_T}\right)^2\right]^2\right\}, \tag{3}$$

where τ_{DS}^{-1} is the scattering rate from dislocation strain, B_D is the magnitude of Burgers vector of the dislocation, γ is the Grüneisen parameter, ν is Poisson's ratio, and v_L and v_T are the longitudinal and transverse phonon velocities, respectively. The fact that dislocations cause the same reduction in thermal conductivity at different temperatures has also been verified by simulations[18,29] and experimental studies.[11]

B. Spectral heat flux

To obtain a quantitative understanding of the phonon–dislocation scattering process, we consider a virtual interface including the dislocation and investigate the spectral heat flux $q(\omega)$ through

TABLE I. Heat flux in selected regions: hot region (H-R), dislocation region (D-R), and cold region (C-R). J_x, J_y, and J_z are the components of the heat flux vector.

	Heat flux	J_x	J_y	J_z
D model	H-R	14.00	−1.4	0.014
	D-R	14.37	−2.18	0.009
	C-R	13.72	−1.4	0.025
P model	H-R	15.18	−0.02	0.014
	D-R	15.20	−0.02	0.014
	C-R	15.18	−0.002	0.004

TABLE II. NEMD results: J_Q is the heat flux, $\partial T/\partial x$ is the temperature gradient, and κ_L is the lattice thermal conductivity calculated by Fourier's law.

	J_Q (GW m^{-2})	$\partial T/\partial x$ (mK nm^{-1})	κ_L (W m^{-1} K^{-1})
D model	14.03	283.6	59.45
P model	15.19	208.1	73.03
D/P ratio	92.36%	…	81.40%

the interface. The heat flowing from the atoms in the **L** group to the atoms in the **R** group as illustrated in the schematic of the NEMD simulation [Fig. 1(b)] is calculated as[22,30]

$$q_{i\to j}(\omega) = -\frac{2}{\omega t}\sum_{\alpha,\beta\in(x,y,z)} \mathrm{Im}\,\langle \tilde{v}_i^{\alpha}(\omega)^{*} K_{ij}^{\alpha\beta} \tilde{v}_j^{\beta}(\omega)\rangle, \tag{4}$$

where ω is the angular frequency, t is the total simulation time, $K_{ij}^{\alpha\beta}$ is the second-order interatomic force constant, and $\tilde{v}_i^{\alpha}(\omega)$ and $\tilde{v}_j^{\beta}(\omega)$ are the discrete Fourier-transformed velocities of atoms i in direction α and atoms j in direction β. The spectral heat flux through the dislocation region is obtained from Eq. (4) by summing over all pairs of atoms in **L** and **R** divided by the cross-sectional area A,

$$q(\omega) = \frac{1}{A}\sum_{i\in\mathbf{L}}\sum_{j\in\mathbf{R}} q_{i\to j}(\omega). \tag{5}$$

The spectral heat flux $q(\omega)$ of the D model (red), P model (blue), and their difference (cyan) are shown in Fig. 4(a). The purple dashed line is the phonon DOS of the P model obtained from the Fourier transform of the velocity autocorrelation function.[31] $q(\omega)$ reveals the contributions from phonons of different frequencies to the heat flux. The curve follows the shape of the phonon DOS, because the contribution to the heat flux from phonons of a given frequency is positively correlated with the total number of phonons of that frequency. $q(\omega)$ decreases between 2.7 and 6.5 THz owing to phonon–dislocation scattering, but it increases in the frequency range from 6.5 to 7.8 THz owing to the frequency deviation of phonons in D model induced by dislocation strain. The cumulative results of $q(\omega)$ are shown in Fig. 4(b), and the total heat flux is 13.51 GW m^{-2} for the D model and 14.46 GW m^{-2} for the P model. The values and their ratio are approximately the same as the NEMD results. By contrast, $q(\omega)$ at frequencies lower than 2.5 THz shows little difference between the two models. This can be understood by considering that low-frequency phonons have relatively long phonon MFPs, and their transport is usually ballistic in nature rather than diffusive as in our finite-length models. Thus, these low-frequency phonons will be not scattered by the dislocation and their energy can pass through the dislocation interface without interference.

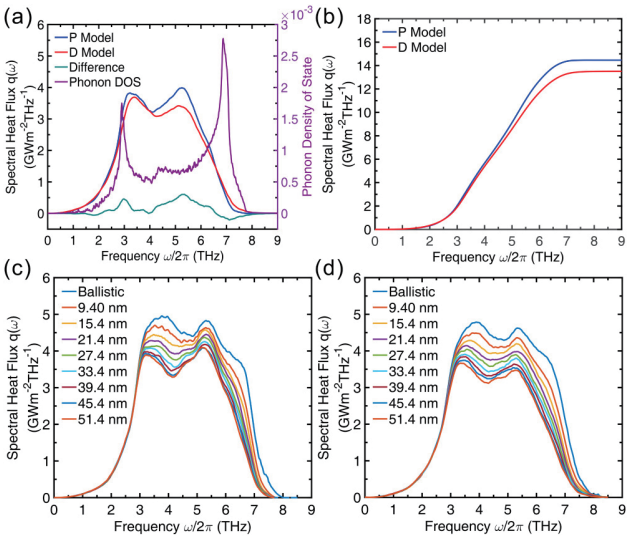

FIG. 4. (a) Frequency-dependent spectral heat flux of the P and D models and their difference. (b) Cumulative heat flux with respect to frequency from (a). (c) Frequency-dependent spectral heat flux of P models of different lengths. (d) Frequency-dependent spectral heat flux of D models of different lengths.

C. Phonon mean free paths

The phonon MFPs $\Lambda(\omega)$ are obtained by fitting the length-dependent spectral heat flux $q(\omega, L)$ to the equation[32,33]

$$q_{(\omega,L)} = \frac{q^0(\omega)}{1 + L/2\Lambda(\omega)}, \tag{6}$$

where $q^0(\omega)$ is the ballistic transmission, denoting the number of modes at frequency ω. Equation (6) has been successfully used to describe the length-dependent heat flux in various systems.[32–35]

We change the system length L_{sys} between the hot and cold baths to calculate $q_{(\omega,L)}$, and the results for the P and D models are plotted in Figs. 4(c) and 4(d), respectively. As expected, when the length of the model increases, the phonons have a higher scattering possibility, which reduces the heat flux. However, ballistic transport can be clearly observed when $f \leq 2.5$ THz, which suggests that the phonon MFPs in this frequency range are much longer than the system scale considered here.[36] The ballistic spectral heat flux and phonon MFPs with 95% confidence interval are shown in Fig. 5(a). We omit the parts of the curves where $q_{(\omega,L)}$ is almost the same to avoid extremely large fitting errors. The phonon MFPs decrease with increasing phonon frequency and are below 1000 nm for phonons with frequency higher than 2.8 THz. The edge dislocation reduces the phonon MFPs in the frequency range from 4.4 to 6.8 THz. The changes in $q(\omega)$ and the decrease in the phonon MFPs reveal the phonon–dislocation scattering. It should be noted that the phonon MFPs of the P model are shorter than those of the D model when $\omega > 7.0$ THz. This is due to the increase in the phonon frequency caused by dislocations in the D model.

The scattering rate τ^{-1} and the phonon MFPs Λ are related by $\tau^{-1} = v_g/\Lambda$, where v_g is the phonon group velocity. Unfortunately, it is impossible to determine the group velocity of our dislocation model owing to the large number of atoms, so v_g is replaced by an average phonon group velocity v_{ave} obtained from a lattice dynamic

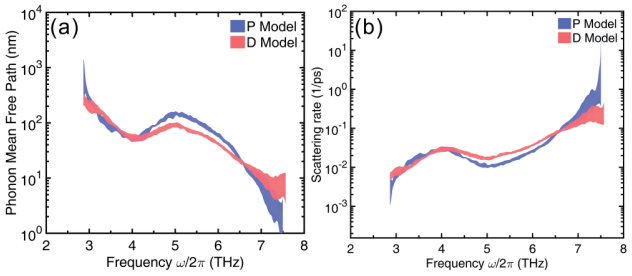

FIG. 5. (a) Phonon MFPs with 95% confidence interval by fitting the length-dependent $q(\omega, L)$ to Eq. (6) and (b) phonon scattering rate with 95% confidence interval by using an average phonon group velocity.

calculation for simplicity. v_{ave} is 1.545 km/s for a perfect iron crystal at 20 K. The scattering rates are then obtained and are shown in Fig. 5(b). The medium-frequency phonons have a higher scattering rate in the dislocation model.

D. Phonon behavior of the dislocation core

To uncover the changes in phonon behavior caused by dislocations, the phonon DOS and eigenmodes of a dislocation dipole model and its corresponding perfect model are obtained. The phonon DOS is shown in Fig. 6(a). The maximum of the phonon frequency in the dislocation dipole model increases, and all the peaks in the DOS of the dislocation dipole model are smoothed compared with the result of the corresponding perfect model. By checking the atomic vibrations of each eigenmode, we find that the atomic motions of the dislocation dipole model exhibit different degrees of localization. Therefore, we investigate the participation ratio (PR) of these modes, which is defined for each mode n as[37]

$$\mathrm{PR}_n = \frac{\left[\sum_i (\vec{e}_{i,n})^2\right]^2}{N \sum_i (\vec{e}_{i,n})^4}, \tag{7}$$

where $\vec{e}_{i,n}$ are the eigenvectors, N is the number of atoms in the system, n is the mode index, and the index i runs over all the atoms

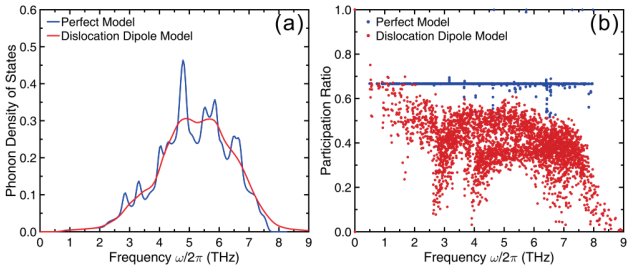

FIG. 6. (a) Phonon DOS and (b) participation ratio of the dislocation dipole model and the corresponding perfect model.

in the supercell. The participation ratio shows the degree of atomic participation in a given mode and is independent of the system size.[38] The value changes from $O(1)$ for spatially extended modes to $O(1/N)$ for a mode completely localized on a single atom.

The PRs of the dislocation dipole model and the corresponding perfect model are shown in Fig. 6(b). We can see that the PRs decrease dramatically in the dislocation dipole model, with a large portion dropping to below 0.1. Vibrational modes with such low PRs have been observed before and have been called "locons."[39] These localized modes cannot deliver thermal energy as efficiently as spatially extended modes, and this may be the main reason that a crystal with dislocations has a smaller κ_L than a perfect crystal.

IV. CONCLUSION

In conclusion, we have investigated the influence of edge dislocations on the κ_L of iron. The value of κ_L calculated by Fourier's law in our NEMD simulations decreased by 18.6% with a 4×10^{15} m^{-2} dislocation density. The results of $q(\omega)$ show that medium-frequency phonons are more likely to be scattered by dislocations, and their phonon MFPs are reduced. From an analysis of eigenmodes, localization of phonons in the dislocation core region is observed in the model with dislocation, and it is the localized phonons that decrease κ_L. Because of the significant phonon contribution to κ of iron-based structural materials in nuclear reactors, such a decrease will cause a degradation of reactor performance and lead to safety flaws. Our study reveals the details of the phonon–dislocation scattering process and may help to interpret the reduced thermal conductivity caused by the dislocations that are generated during the service life of iron-based structural materials.

ACKNOWLEDGMENTS

Y.D.S. thanks Dr. Shiyao Liu for polishing the language. Simulations were performed with computing resources granted by the National Supercomputer Center in Tianjin under Project TianHe-1(A). Research reported in this publication was supported by the Basic Science Center Project of NSFC under grant No. 51788104 and by the Tsinghua National Laboratory for Information Science and Technology. Research reported in this publication was supported, in part, by the NSF (Award No. 1905775) and the SC EPSCoR/IDeA Program under NSF No. OIA-1655740 via SC EPSCoR/IDeA 19-SA06 and GEAR-CRP2019 19-GC02. The views, perspective, and content do not necessarily represent the official views of the SC EPSCoR/IDeA Program nor those of the NSF.

REFERENCES

[1]S. J. Zinkle and J. T. Busby, Mater. Today **12**, 12 (2009).
[2]P. Klemens and R. Williams, Int. Metals Rev. **31**, 197 (1986).
[3]T. M. Tritt, *Thermal Conductivity: Theory, Properties, and Applications* (Springer, 2005).
[4]W. Fulkerson, J. Moore, and D. McElroy, J. Appl. Phys. **37**, 2639 (1966).
[5]R. Williams, R. Graves, F. Weaver, and D. Yarbrough, J. Appl. Phys. **62**, 2778 (1987).
[6]J. Callaway, Phys. Rev. **122**, 787 (1961).
[7]C. Walker and R. Pohl, Phys. Rev. **131**, 1433 (1963).
[8]M. Zhao, W. Pan, C. Wan, Z. Qu, Z. Li, and J. Yang, J. Eur. Ceram. Soc. **37**, 1 (2017).

[9]P. Schelling, S. Phillpot, and P. Keblinski, Appl. Phys. Lett. **80**, 2484 (2002).
[10]H. Zhao and J. Freund, J. Appl. Phys. **97**, 024903 (2005).
[11]S. I. Kim, K. H. Lee, H. A. Mun, H. S. Kim, S. W. Hwang, J. W. Roh, D. J. Yang, W. H. Shin, X. S. Li, and Y. H. Lee, Science **348**, 109 (2015).
[12]J. He, S. N. Girard, M. G. Kanatzidis, and V. P. Dravid, Adv. Funct. Mater. **20**, 764 (2010).
[13]Z. Chen, B. Ge, W. Li, S. Lin, J. Shen, Y. Chang, R. Hanus, G. J. Snyder, and Y. Pei, Nat. Commun. **8**, 13828 (2017).
[14]Y. Pan, U. Aydemir, J. A. Grovogui, I. T. Witting, R. Hanus, Y. Xu, J. Wu, C.-F. Wu, F.-H. Sun, and H.-L. Zhuang, Adv. Mater. **30**, 1802016 (2018).
[15]B. Sun, G. Haunschild, C. Polanco, L. Lindsay, G. Koblmüller, Y. K. Koh *et al.*, Nat. Mater. **18**, 136 (2019).
[16]S. Xiong, J. Ma, S. Volz, and T. Dumitrică, Small **10**, 1756 (2014).
[17]Y. Ni, S. Xiong, S. Volz, and T. Dumitrică, Phys. Rev. Lett. **113**, 124301 (2014).
[18]K. Termentzidis, M. Isaiev, A. Salnikova, I. Belabbas, D. Lacroix, and J. Kioseoglou, Phys. Chem. Chem. Phys. **20**, 5159 (2018).
[19]T. Wang, J. Carrete, A. van Roekeghem, N. Mingo, and G. K. Madsen, Phys. Rev. B **95**, 245304 (2017).
[20]M. Li, Z. Ding, Q. Meng, J. Zhou, Y. Zhu, H. Liu, M. S. Dresselhaus, and G. Chen, Nano Lett. **17**, 1587 (2017).
[21]R. Hanus, M. T. Agne, A. J. Rettie, Z. Chen, G. Tan, D. Y. Chung, M. G. Kanatzidis, Y. Pei, P. W. Voorhees, and G. J. Snyder, Adv. Mater. **31**, 1900108 (2019).
[22]K. Sääskilahti, J. Oksanen, J. Tulkki, and S. Volz, Phys. Rev. B **90**, 134312 (2014).
[23]Y. Zhou, X. Zhang, and M. Hu, Phys. Rev. B **92**, 195204 (2015).
[24]Y. Zhou and M. Hu, Phys. Rev. B **92**, 195205 (2015).
[25]S. Plimpton, J. Comput. Phys. **117**, 1 (1995).
[26]L. Proville, D. Rodney, and M.-C. Marinica, Nat. Mater. **11**, 845 (2012).
[27]A. Togo and I. Tanaka, Scr. Mater. **108**, 1 (2015).
[28]L. Wang, *Molecular Dynamics: Theoretical Developments and Applications in Nanotechnology and Energy* [Books on Demand (BoD), 2012].
[29]H.-S. Kim, S. D. Kang, Y. Tang, R. Hanus, and G. J. Snyder, Mater. Horiz. **3**, 234 (2016).
[30]Y. Zhou, X. Zhang, and M. Hu, Nanoscale **8**, 1994 (2016).
[31]H. Jobic, K. S. Smirnov, and D. Bougeard, Chem. Phys. Lett. **344**, 147 (2001).
[32]K. Sääskilahti, J. Oksanen, S. Volz, and J. Tulkki, Phys. Rev. B **91**, 115426 (2015).
[33]K. Sääskilahti, J. Oksanen, J. Tulkki, and S. Volz, Phys. Rev. E **93**, 052141 (2016).
[34]S. Xiong, K. Sääskilahti, Y. A. Kosevich, H. Han, D. Donadio, and S. Volz, Phys. Rev. Lett. **117**, 025503 (2016).
[35]I. Savić, N. Mingo, and D. A. Stewart, Phys. Rev. Lett. **101**, 165502 (2008).
[36]J. S. Kang, M. Li, H. Wu, H. Nguyen, and Y. Hu, Science **361**, 575 (2018).
[37]A. Bodapati, P. K. Schelling, S. R. Phillpot, and P. Keblinski, Phys. Rev. B **74**, 245207 (2006).
[38]X. Zhang, M. Hu, K. P. Giapis, and D. Poulikakos, J. Heat Transfer **134**, 102402 (2012).
[39]P. B. Allen and J. L. Feldman, Phys. Rev. B **48**, 12581 (1993).